Corner- versus face-sharing octahedra in $A\mathrm{MnO_3}$ perovskites (A=Ca, Sr, and Ba)

Rune Søndenå, Svein Stølen,* and P. Ravindran
Department of Chemistry and Centre for Materials Science and Nanotechnology, University of Oslo, Postbox 1033 Blindern, N-0315 Oslo, Norway

Tor Grande
Department of Materials Science and Engineering, Norwegian University of Science and Technology, N-7491 Trondheim, Norway

Neil L. Allan
School of Chemistry, University of Bristol, Cantock's Close, Bristol BS8 1TS, United Kingdom
(Received 20 December 2006; revised manuscript received 15 March 2007; published 14 May 2007)

The electronic structure of the series of perovskites $A\mathrm{MnO_3}$ (A=Ca,Sr,Ba) is examined with the aid of density-functional calculations. A range of possible crystal structures is examined for each compound, and in each case the calculated lowest-energy structure is that observed at low temperature. The factors that control the variation in structure with the alkaline-earth ion A^{2+} are discussed. $\mathrm{CaMnO_3}$ consists of corner-sharing octahedra but is orthorhombically distorted consistent with $\mathrm{Ca^{2+}}$ being too small for the 12-fold site within a perfect cubic $\mathrm{MnO_6}$ polyhedral framework. When the size of the alkaline-earth cation increases, a transformation from corner-sharing to face-sharing octahedra is induced since the alkaline-earth cation now becomes too large for the 12-fold site. While $\mathrm{SrMnO_3}$ at 0 K has the four-layered hexagonal ($4H$) structure with corner-sharing $\mathrm{Mn_2O_9}$ dimers, $\mathrm{BaMnO_3}$ at 0 K adopts the two-layered hexagonal ($2H$) structure with infinite chains of face-sharing octahedra. The Mn charge is much lower than the conventional ionic model charge due to Mn-O covalence, and this reduces the Mn-Mn repulsion and favors sharing of the octahedral faces. We see no evidence for direct Mn-Mn metal bonding which has often been invoked to rationalize the adoption of this type of structure. We also discuss the atomistic origins of acid-base stabilization of ternary oxides from their binary constituents. A link between cation size and acid-base properties is suggested for $A\mathrm{MnO_3}$.

DOI: 10.1103/PhysRevB.75.184105 PACS number(s): 61.50.Ah, 61.50.Lt, 61.50.Ks, 64.70.Kb

I. INTRODUCTION

Ideal perovskites have the general formula ABX_3, where the A-site cations are typically larger than the B-site cations and similar in size to the X-site anions. While the A-site cations are surrounded by 12 anions in cubo-octahedral coordination, the B-site cations are surrounded by six anions in octahedral coordination [see Fig. 1(a)]. The X-site anions are coordinated by two B-site cations and four A-site cations. Ideal perovskites adopt the space-group $Pm\bar{3}m$, and $\mathrm{CaTiO_3}$ is commonly regarded as the archetypical cubic perovskite. While the ideal perovskite structure is cubic, the majority of perovskites are distorted due to rotation or tilting of regular, rigid BX_6 octahedra or due to a distortion of the BX_6 octahedra themselves. Tilting of the octahedra occurs when the size of the A cation is too small for the 12-fold site within a BX_6 polyhedral framework. This tilting of the BX_6 polyhedra necessarily induces a distortion of the AX_{12} polyhedra which eventually results in a decrease in the A-cation coordination number. The rotation or tilting does not disrupt the corner-sharing connectivity present in the ideal cubic perovskite.

The structure of a perovskite-related oxide can, to some extent, be predicted from the tolerance factor t

$$t = (r_A + r_X)/\sqrt{2}(r_B + r_X), \tag{1}$$

where r_A, r_B, and r_X are the ionic radii of the ions A, B, and X, respectively. $t=1$ corresponds to an "ideal" cubic perovskite, while smaller values of t ($t<0.88$) correspond to an orthorhombic distortion. A tolerance factor larger than unity, on the other hand, implies that the A-site cations are too large to be accommodated in the A-site of the BX_3 framework, and hexagonal perovskites are formed. In these, some octahedra share faces, and chains are formed along the hexagonal c axis. Face-sharing octahedra have B-B distances close to those in metallic B, thus increasing the electrostatic repulsion between the B-site cations. As a compromise, hexagonal stacking is introduced in stages with increasing size of the A-site cation. Polyhedral representations of the $4H$ and $2H$ polymorphs are given in Figs. 1(b) and 1(c), respectively. While the two-layered ($2H$)-hexagonal structure contains face-sharing octahedra only, the four-layered ($4H$)-hexagonal structure may be regarded as intermediate, containing both corner- and face-sharing octahedra.

The majority of the hexagonal perovskites contain large alkali- or alkaline-earth metals on the A-site and transition metals on the B-site. The alkaline-earth manganese oxides, $A\mathrm{MnO_3}$, show the importance of size on stability well. The ionic radius of the 12-coordinated alkaline-earth ion increases from $\mathrm{Ca^{2+}}$ ($r_{\mathrm{Ca^{2+}}}=1.35$ Å) to $\mathrm{Sr^{2+}}$ ($r_{\mathrm{Sr^{2+}}}=1.44$ Å) and $\mathrm{Ba^{2+}}$ ($r_{\mathrm{Ba^{2+}}}=1.60$ Å) (Ref. 1), and while $\mathrm{CaMnO_3}$ forms an orthorhombic variant of the ideal cubic structure,[2] $\mathrm{BaMnO_3}$ forms a hexagonal $2H$ structure (space-group $P6_3/mmc$).[3] $\mathrm{SrMnO_3}$, containing intermediately sized $\mathrm{Sr^{2+}}$ ions, is a rare example of a compound taking both a cubic and a hexagonal perovskite structure.[4–6] The $4H$-hexagonal polymorph (space-group $P6_3/mmc$) is stable up to about 1035 °C where it transforms to a cubic high-temperature modification with only a small enthalpy of transition, about 6 kJ $\mathrm{mol^{-7}}$.[7]

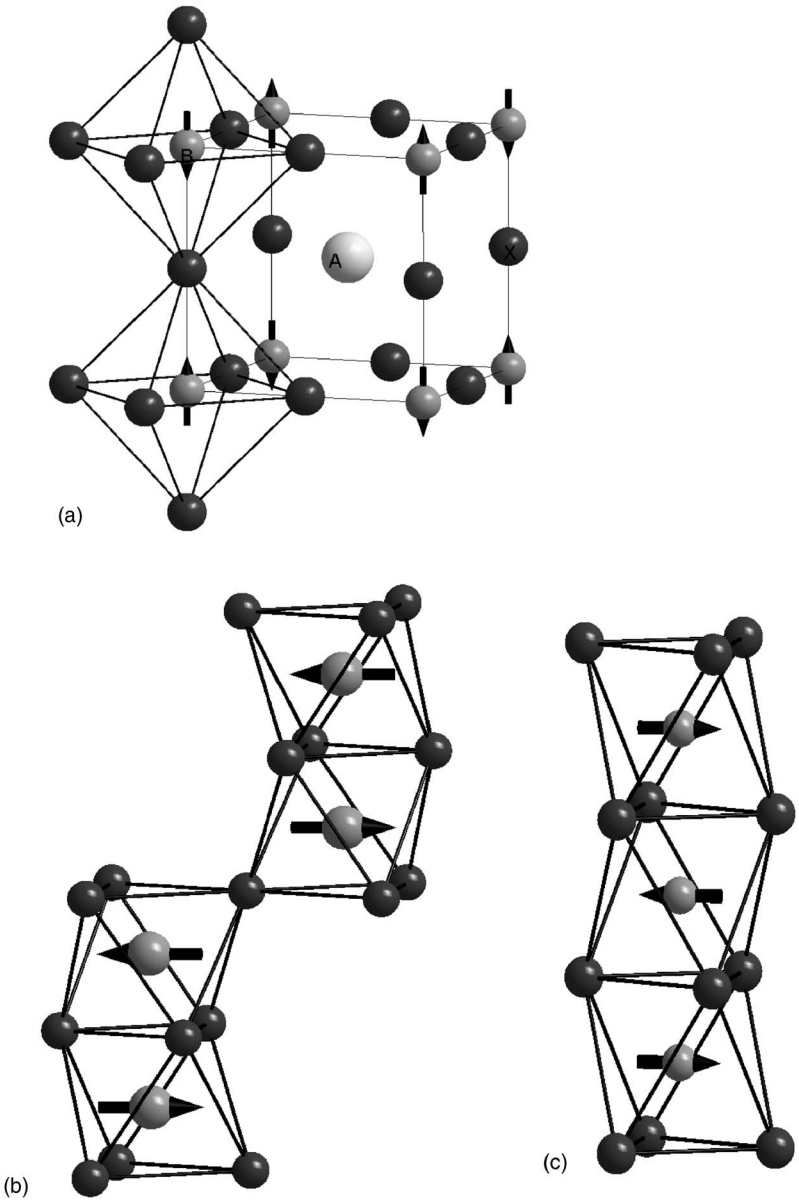

FIG. 1. Polyhedral representations of (a) the ideal cubic perovskite (b) the four-layered hexagonal perovskite and (c) the two-layered hexagonal perovskite structures.

Temperature-induced transitions which increase the fraction of corner-sharing octahedra are observed also for $BaMnO_3$.[8,9]

In a recent paper, we discussed the electronic and magnetic structures of cubic and 4*H*-hexagonal $SrMnO_3$.[10] While the bonding interactions involving Sr were found to be mainly ionic, there is a significant covalent contribution to the Mn-O bond. It was suggested that this covalency is important for the stabilization of the hexagonal structure compared to the cubic polymorph. Two additional related factors were discussed: the displacement of the Mn atoms in the face-sharing octahedra away from the center of the octahedra along the *c* axis of the hexagonal structure and the charge transfer giving a lower charge on oxygen atoms in the oxygen triangle of the shared face compared to those in the plane where the octahedra share corners. The combination of these two factors results in a contraction of the oxygen triangle that to some extent shields the repulsive interaction between the manganese atoms in the Mn_2O_9 dimer. In this paper, electronic band-structure calculations for $AMnO_3$, where *A* =Ca, Sr, and Ba, are reported. The ideal cubic, the 2*H*- and the 4*H*-hexagonal modifications (see Fig. 1) are considered for all three compounds. In addition, the orthorhombically distorted structure observed for $CaMnO_3$ is also considered. Electronic structure, bonding, and the main driving forces controlling corner versus face sharing of octahedra are discussed. We also discuss the microscopic origins of acid-base stabilization of ternary oxides from their binary constituents.

II. COMPUTATIONAL DETAILS

For most of our calculations, we have used the projector augmented wave[11] implementation of the Vienna *ab initio* simulation package.[12–14] The self-consistent calculations are performed using the generalized gradient approximation (GGA).[15] The cutoff energy for the plane-wave basis is 500 eV. Periodic unit cells containing 10 atoms (2 f.u.) are used for the cubic and 2*H* structures, while the 4*H* and ortho-

TABLE I. Fractional atomic coordinates for the 4*H*- and 2*H*-hexagonal structures.

	Wyckoff	*x*	*y*	*z*
		$4H$-$P6_3/mmc$		
A1	2*a*	0	0	0
A2	2*c*	1/3	2/3	1/4
Mn	4*f*	1/3	2/3	z_{Mn}
O1	6*g*	0	0	1/2
O2	6*h*	$-x_{\mathrm{O2}}$	$-2x_{\mathrm{O2}}$	1/4
		$2H$-$P6_3/mmc$		
A	2*d*	1/3	2/3	3/4
Mn	2*a*	0	0	0
O	6*h*	x_{O}	$2x_{\mathrm{O2}}$	1/4

rhombic cells have 20 atoms (4 f.u.). To ensure high accuracy, the *k*-point density and the plane-wave cutoff energy are increased until convergence ($19\times19\times19$ for cubic, $13\times13\times8$ for 4*H*, $13\times13\times13$ for 2*H*, and $14\times10\times14$ for orthorhombic cells). The chosen parameters give approximately the same *k*-point density in the reciprocal space. The Monkhorst-Pack mesh is used for the cubic and orthorhombic unit cells, while a Γ-centered *k*-point mesh is used for the hexagonal cells. All calculations are spin polarized; majority- and minority-spin electrons are treated separately.

The atomic coordinates for the 2*H* and 4*H* polymorphs are given in Table I. Several magnetically ordered structures are, in general, possible both for cubic and the hexagonal perovskites. We have used the *G*-type antiferromagnetic order [see Fig. 1(a)] observed for cubic $SrMnO_3$ (Ref. 10) for all the cubic structures (ten atom unit cells). An antiferromagnetic configuration with alternating spins along the *c* axis (both within the Mn_2O_9-dimers and between the corner-sharing MnO_6 octahedra) and with spins parallel to the *a* axis is used for the 4*H* modification, see Fig. 1(b). This modification has been found experimentally for 4*H* $BaMnO_3$ (Ref. 16) and $Ba_{0.1}Sr_{0.9}MnO_{2.96}$ (Ref. 17) and theoretically for 4*H* $SrMnO_3$.[10] For 2*H* $AMnO_3$ a configuration (ten atoms) with antiferromagnetic coupling along the *c* axis is used [see Fig. 1(c)]. This simplification makes the computational cost of the calculations feasible. Experiments show that the spin directions associated with the Mn chains at $(1/3\ 2/3\ z)$ and $(2/3\ 1/3\ z)$ are rotated ±120° with respect to the chain at $(0\ 0\ z)$.[18]

The enthalpies of formation of the ternary oxides from the binary oxides

$$AO + MnO_2 \rightarrow AMnO_3 \tag{2}$$

are given by

$$\Delta_{f,\mathrm{oxides}}H^o(AMnO_3) = \Delta_f H^o(AMnO_3) - \Delta_f H^o(AO) - \Delta_f H^o(MnO_2). \tag{3}$$

Hence, total energies are also calculated for CaO, SrO, and BaO (space-group $Fm\bar{3}m$),[19] and MnO_2 (Ref. 20) (space-group $P4_2/mnm$). In the latter case, the magnetic configuration is too complex,[20] and a slightly simpler antiferromagnetic structure, in which the two Mn atoms of the unit cell are aligned antiparallel, is considered.[21] This simplification does not affect the calculated enthalpy of reaction (2) to any appreciable extent due to the small energy difference between these magnetic orderings.

III. RESULTS AND DISCUSSION

The calculated unit-cell dimensions and magnetic moments of the different crystal structures considered for $CaMnO_3$, $SrMnO_3$, and $BaMnO_3$ are presented in Table II. Some experimental results from the literature are also given in the table. For each structure, the unit-cell dimensions as well as the atomic coordinates are optimized.

The magnetic moment is largely independent of the crystal structure and of the alkaline-earth ion, varying from 2.40 to $2.52\mu_B$/Mn. This agrees well with available experimental values for the oxides considered here and related compounds. Also the calculated unit-cell dimensions for the lowest-energy modification are in good agreement with the experimental values. In general, GGA overestimates equilibrium volumes, and agreement with experiment within 2% is considered good. Calculated and experimental atomic coordinates for the 4*H* and 2*H* polymorphs are given in Table III. Excellent agreement is obtained.

Relative polymorph stability in agreement with experiment is obtained for all three compounds, where data are available. Figure 2 shows the calculated enthalpy of formation of the different polymorphs from their binary constituents for each compound. The values are also given in Table II. Increasing the size of the alkaline-earth cation induces a transition from corner sharing to face sharing of octahedra. The lowest-energy structure for $CaMnO_3$ is an orthorhombic distorted variant of the ideal cubic structure. $SrMnO_3$ with the intermediately sized alkaline-earth cation preferentially adopts the 4*H* structure with corner-sharing Mn_2O_9 dimers, consisting of two octahedra sharing a face. $BaMnO_3$ takes the 2*H* polymorph in which there is only face sharing of MnO_6 octahedra. The only experimental value for the enthalpy of formation of $SrMnO_3$ (−99.8 kJ mol^{-1} from the binary oxides)[7,26] we have been able to find is in good agreement with the calculated value (see Fig. 2). A value determined in similar experiments for $CaMnO_3$ (−89.0 kJ mol^{-1})[7,26] is about ≈37 kJ mol^{-1} more negative than that calculated.

A. Electronic structure and bonding

The total electronic density of states (DoS) and the Mn and O contributions to these are given in Fig. 3 for the different polymorphs considered for $CaMnO_3$ [Fig. 3(a)], $SrMnO_3$ [Fig. 3(b)], and $BaMnO_3$ [Fig. 3(c)]. The DoS contribution from the alkaline-earth ion is negligibly small near the Fermi energy in all cases, indicating a high degree of ionic bonding between alkaline-earth ion and the host lattice. All structures considered for the three compounds are insulators; the band gaps are given in Table IV. It is worth noting that the method used here usually underestimates the band

TABLE II. Unit-cell dimensions, magnetic moments, and total energy of the different polymorphs considered for $AMnO_3$ (A=Ca, Sr, and Ba).

Compound	modification	a (Å)	b (Å)	c (Å)	Magnetic moment (μ_B)	Energy (meV)
$CaMnO_3$	Orthorombic calc.	5.3298	7.4873	5.2818	2.52	−287
	Orthorombic expt.[a]	5.2819(1)	7.4547(2)	5.2658(1)		
	Cubic calc.	3.7584			2.45	0
	4*H* calc.	5.3488		9.0216	2.44	−18
	2*H* calc.	5.3008		4.7420	2.38	239
$SrMnO_3$	Cubic calc.	3.8244			2.47	0
	Cubic expt.[b]	3.80(2)			2.6(2)	
	4*H* calc.	5.4893		9.1143	2.47	−251
	4*H* expt.[c]	5.4434(2)		9.0704(1)		
	2*H* calc.	5.5053		4.7711	2.40	−111
$BaMnO_3$	Cubic calc.	3.9361			2.49	0
	4*H* calc.	5.6936		9.2827	2.50	−690
	HT 4*H* expt.[d]	5.669(3)		9.375(15)		
	4*H* expt.[e]	5.62732(8)		9.2080(1)	2.71(2)	
	2*H* calc.	5.7781		4.8217	2.42	−850
	2*H* expt.[f]	5.6691(2)		4.8148(2)	1.31(5)	
	2*H* expt.[g]	5.695		4.812		
	2*H* expt.[h]	5.67(5)		4.70(8)		

[a]Reference 22.
[b]Reference 23.
[c]Reference 24.
[d]Reference 25.
[e]Reference 16.
[f]Reference 18.
[g]Reference 3.
[h]Reference 4.

gap. Close to E_F the density-of-states contribution from manganese dominates for all compounds and structures, but there are also O contributions. The conduction band is dominated by manganese d states, and the band gap is of an intermediate character having both p-d charge-transfer and d-d Mott-Hubbard characteristics.

The previous study of cubic and 4*H* $SrMnO_3$ clearly showed several different features of the band structures that point to significant covalent contributions to the bonding.[10] This interpretation is further supported by the present calculations. First of all, the manganese and oxygen DoS contributions overlap in the valence band for all polymorphs for all three compounds, indicating a degree of covalency of the bonds. In the previous paper on $SrMnO_3$, this interpretation was supported by a crystal orbital Hamiltonian population analysis which identified bonding, antibonding, and nonbonding interactions between Mn and O in cubic $SrMnO_3$.[10] Furthermore, even though Mn in the antiferromagnetic ground state formally has a d^3 configuration (three unpaired spins in an octahedral crystal field), on each Mn there is a significant population of minority-spin states in the valence band. If the bonding was purely ionic Mn^{4+} (d^3), there would be no minority-spin contributions from the Mn d orbitals in the DoS in the right-hand frames in Fig. 3. Also, the calculated magnetic moments of manganese deviate from those expected for a purely ionic case (three unpaired spins).

The charges on the ions derived from a Bader charge population analysis[27] also indicate partial covalency. While the charges obtained for the A and Mn ions are about +1.6 and +2.0 for all the compounds in all the structures, the charges on the oxygen atoms vary somewhat. For the 4*H* polymorphs, there is a difference between the charges of the O ions in the face-sharing triangle (−1.15) and the O ions corner shared (−1.27) between two MnO_6 octahedra. On av-

TABLE III. Calculated fractional atomic coordinates for 4*H* and 2*H* $AMnO_3$ (A=Ca, Sr, and Ba).

	"Ideal"	$CaMnO_3$	$SrMnO_3$	$BaMnO_3$
		4*H*		
z_{Mn} calc.	5/8	0.6142	0.6129	0.6122
z_{Mn} expt.			0.6122(5)[a]	0.60855(9)[b]
x_{O2} calc.	1/6	0.1752	0.1805	0.1881
x_{O2} expt.			0.1807(2)[a]	0.18677(2)[b]
		2*H*		
x_O calc.	1/6	0.1612	0.1559	0.1487
x_O expt.				0.14950(5)[c]

[a]Reference 24.
[b]Reference 16.
[c]Reference 18.

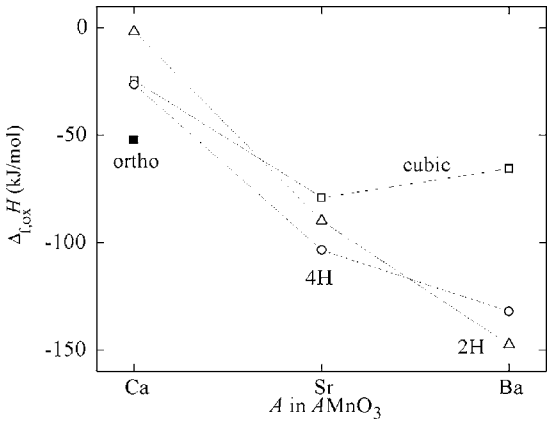

FIG. 2. The enthalpy of formation of ternary oxides from their binary constituents. Squares represent the cubic polymorph, circles the 4*H* polymorph, and triangles the 2*H* polymorph. The filled symbol denotes orthorhombic $CaMnO_3$.

erage, the O charges are ≈−1.2. It can be noted that the present results agree with Mulliken charges for $CaMnO_3$ calculated using the periodic Hartree-Fock theory. In that case, the charges reported for Ca, Mn, and O were 1.86, 2.17, and −1.34, respectively.[2]

A final feature is present in the orbital-resolved DoS for cubic $AMnO_3$. The local octahedral coordination of the Mn atoms in cubic $AMnO_3$ gives rise to two- and threefold degenerate e_g and t_{2g} Mn *d* orbitals due to crystal-field effects. In manganese oxides (i.e., MnO) the on-site exchange splitting is larger than the ligand field splitting, and both the valence band (VB) and the conduction band have a mixed e_g/t_{2g}-character.[28,29] Crystal-field effects alone would raise the energy of the e_g orbitals relative to the t_{2g} since the e_g orbitals point directly towards the neighboring O atoms. In the present case, however, the covalent character of the manganese-oxygen σ bond lowers the energy of some of the occupied e_g states; t_{2g} orbitals form weaker π manganese-oxygen bonds. As a result such e_g states are lower in energy than the t_{2g} states in the VB in cubic $AMnO_3$ (see Fig. 4). The difference in energy between the bottom of the t_{2g} and e_g states and t_{2g} shift increases from $CaMnO_3$ to $BaMnO_3$, consistent with an increasing degree of Mn-O covalent σ bonding.

B. Enthalpy of formation and acid-base arguments

The enthalpy of formation of a ternary oxide (such as ABO_3) from the binary constituent oxides (like *A*O and BO_2) reflects the strength and number of the chemical bonds in the ternary oxide relative to those in the binary oxides. $\Delta_{f,\text{oxides}}H_m^o$ is often interpreted qualitatively in terms of factors related to oxide ion transfer between the constituent oxides, i.e., acidity/basicity.[30,31] The larger the difference in acidity of A_mO_n and B_xO_y, the more exothermic is the enthalpy of formation of the ternary oxide from its binary constituents. While *s*-block oxides are usually basic, the *p*-block oxides are acidic. The basicity of the alkaline-earth oxides increases down the group, i.e., CaO < SrO < BaO. Thus, when combining these binary alkaline-earth oxides with a

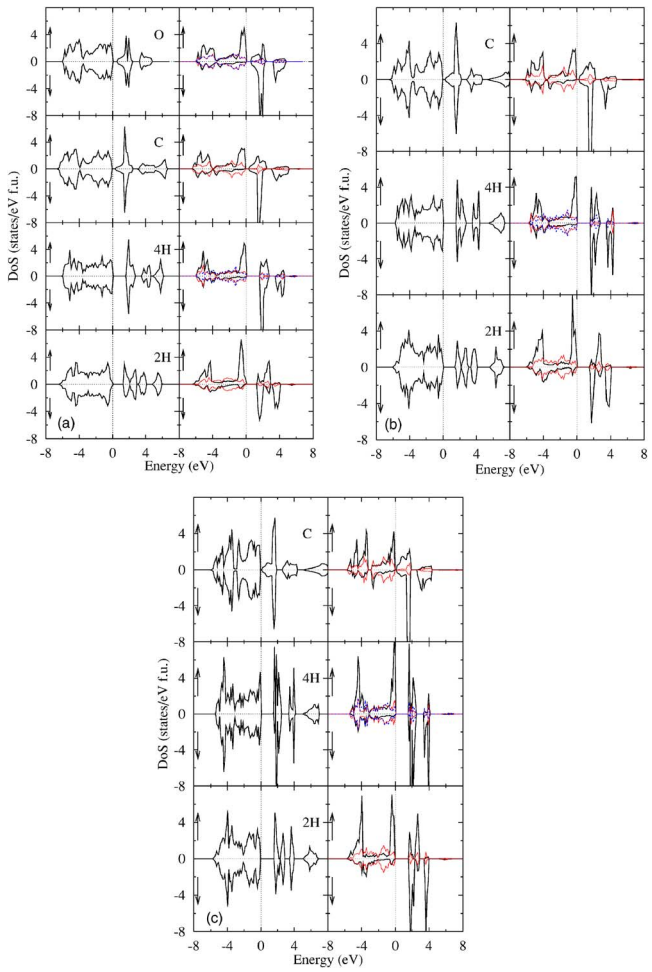

FIG. 3. (Color online) The electronic density of states for (a) $CaMnO_3$, (b) $SrMnO_3$, and (c) $BaMnO_3$. The total densities of states are given on the left-hand side of the figures. The Mn and O contributions to the densities of state are given on the right-hand side of the figure. The Mn contributions are represented by thick black lines, while the oxygen contributions are given by thin red (solid) and (for 4*H* polymorphs) blue (dashed) lines. For 4*H* polymorphs, the red curves are for corner-sharing oxygens, and blue curves for face-sharing oxygens.

given oxide such as MnO_2, the enthalpy of formation of $BaMnO_3$ from the constituent oxides is expected to be more negative than that of $SrMnO_3$, for which, similarly, $\Delta_{f,\text{oxides}}H_m^o$ is expected to be more negative than for $CaMnO_3$.

Our *ab initio* calculations allow us to calculate these enthalpies of reaction for comparison with the acid-base model. The enthalpy of formation of the 2*H* ternary oxides from

TABLE IV. Calculated band gaps (eV) for the different polymorphs considered for $AMnO_3$ (*A*=Ca, Sr, and Ba).

	Orthorombic	Cubic	4*H*	2*H*
$CaMnO_3$	0.70	0.46	1.77	1.43
$SrMnO_3$		0.30	1.72	1.57
$BaMnO_3$		0.21	1.64	1.68

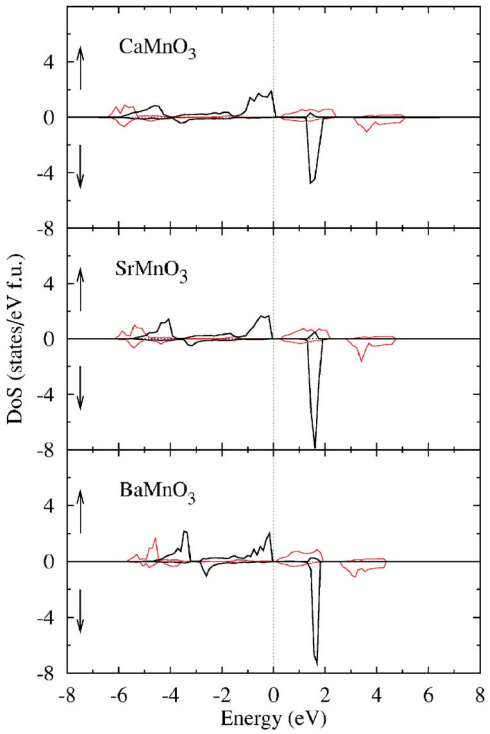

FIG. 4. (Color online) The t_{2g}-e_g decomposed electronic density of state (d-orbitals only) of manganese in G-type AF cubic $A\mathrm{MnO_3}$. The t_{2g} contribution is given in black (thick line), and the e_g in red (thin line).

their binary constituents increases from -1.6 kJ mol^{-1} for $\mathrm{CaMnO_3}$ to -90 kJ mol^{-1} for $\mathrm{SrMnO_3}$ and to -148 kJ mol^{-1} for $\mathrm{BaMnO_3}$. Hence, the trend expected from the usual acid-base argument is obtained. The enthalpy of formation of the $2H$ ternary oxides from their binary constituents are visualized in Fig. 5 as the difference between the enthalpies of formation of the ternary $2H$ oxides and the sum of the enthalpies of formation of the constituent binary oxides. Data for the binary oxides (from the elements) are taken from experiment.[32] The enthalpy of formation of the ternary oxides (from the elements) is obtained by adding the presently calculated $\Delta_{f,\mathrm{oxides}}H^{\mathrm{o}}_m$ to the enthalpy of formation (from the elements) of the binary oxides.

The first question is the extent to which this trend is visible in the electronic density of states of the compounds involved. The total electronic densities of states for $2H$ $\mathrm{CaMnO_3}$, $\mathrm{SrMnO_3}$, and $\mathrm{BaMnO_3}$ are given in Fig. 6. For all three compounds, the bands from -19 to -17 eV are from O $2s$ and the changes in these from Ca to Ba are minor. There is a large change in the position of the narrow bands due to the semicore alkaline-earth p-electron states from -21 eV for Ca $3p$ states in $\mathrm{CaMnO_3}$ via -16 eV for Sr $4p$ states in $\mathrm{SrMnO_3}$ to -11 eV for Ba $5p$ states in $\mathrm{BaMnO_3}$. These narrow bands are not expected to participate in bonding, as confirmed by the minimal contribution to the oxygen DoS at the same energies. The remaining part of the electronic DoS of the valence band is that close to E_F, which is mainly due to Mn and O contributions. This part becomes slightly narrower from $\mathrm{CaMnO_3}$ to $\mathrm{BaMnO_3}$. Thus, there is only a small variation between the electronic densities of states of the ternary

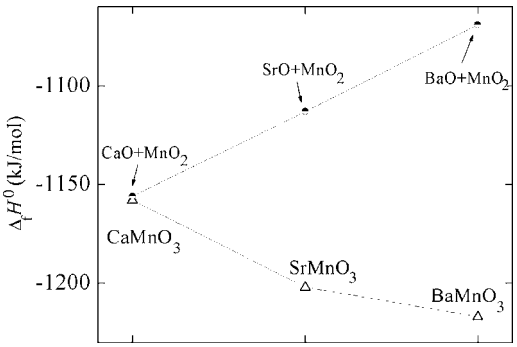

FIG. 5. The sum of the enthalpy of formation (from the elements) of the binary alkaline-earth oxides and $\mathrm{MnO_2}$ (Ref. 28). The enthalpy of formation of ternary $2H$ $A\mathrm{MnO_3}$ from the elements are also included to visualize the physical meaning of $\Delta_{f,\mathrm{oxides}}H^{\mathrm{o}}_m$. The enthalpy of formation of the ternary oxides from the elements is obtained by adding the presently calculated $\Delta_{f,\mathrm{oxides}}H^{\mathrm{o}}_m$ to the enthalpy of formation for the binary oxides (Ref. 28).

oxides. Let us now consider instead the changes in the electronic structure due to the formation of the $2H$ oxides from their binary constituent oxides. Figure 7 compares site-decomposed electronic DoS for $2H$ $A\mathrm{MnO_3}$ with the corresponding DoS for the binary constituent oxides, neglecting the lower-energy states not contributing to bonding. One significant difference between the binary and ternary oxides is evident. In all three cases the Mn and O DoS are narrower for the ternary oxide than for $\mathrm{MnO_2}$, and as we have already commented the width also decreases slightly from $\mathrm{CaMnO_3}$ to $\mathrm{SrMnO_3}$ to $\mathrm{BaMnO_3}$. The contribution from the alkaline-earth states is, on the other hand, much narrower for the AO oxides than for the ternary oxides. Bonding in binary AO is

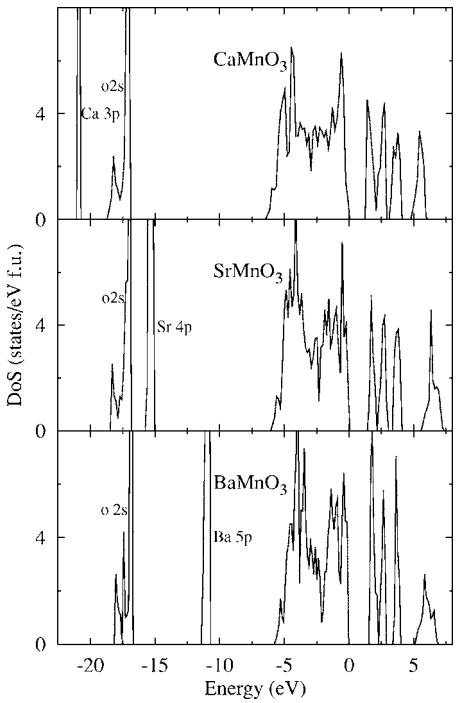

FIG. 6. The total electronic density of states (spin up and spin down) for $2H$ $A\mathrm{MnO_3}$.

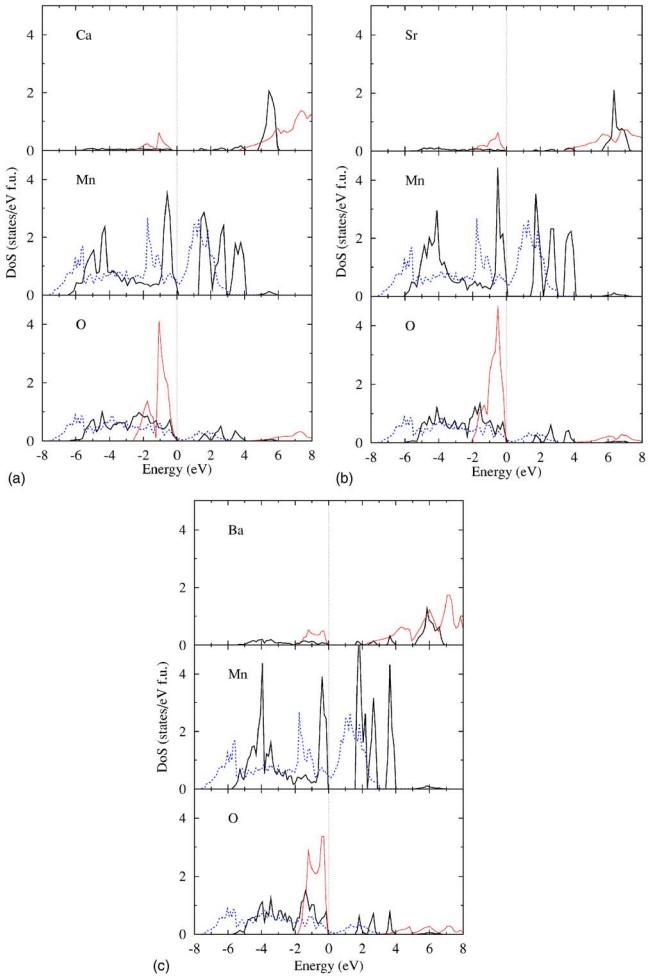

FIG. 7. (Color online) The site-decomposed electronic density of states for the 2*H* ternary oxides and the corresponding binary oxides: (a) CaO, MnO_2, and $CaMnO_3$; (b) SrO, MnO_2, and $SrMnO_3$; and (c) BaO, MnO_2, and $BaMnO_3$. Thick black lines represent the ternary oxide, thin red lines the *A*O oxides, and dotted lines MnO_2.

indicated by the overlap of *A* and O states in the valence-band region close to E_F. The width of the *A*-valence band decreases going from Ca to Ba, indicating less overlap and weaker *A*-O covalent bonding. In conclusion, no evident correlation between the electronic band structures of the ternary and binary oxides and the enthalpy of formation from the binary constituent oxides is found.

Alternatively, consider cation size. The variation in $\Delta_{f,\text{oxides}}H_m^\circ$ for the ternary oxides is dominated by the difference in lattice enthalpy of $AMnO_3$ and $AO+MnO_2$ [see Eq. (3)]. This difference becomes more negative from Ca to Ba. All three binary alkaline-earth monoxides take the NaCl structure. In the simplest ionic picture, their lattice energy is inversely proportional to the interatomic distance which increases from 2.40 Å in CaO to 2.56 Å in SrO and 2.76 Å in BaO. On this basis alone, the lattice energy of BaO is expected to be approximately 15% lower than that of CaO, and the lattice energy contribution dominates the variation in the enthalpy of formation of the binary oxides from the elements, which becomes less exothermic from CaO to BaO (Fig. 5). Unlike the enthalpy of formation of the binary oxides from the elements, the enthalpy of formation of the ternary oxides from the binary oxides becomes more exothermic from Ca to Ba. This also is a size-related effect. While Ca^{2+} is too small for the A site of the 2*H* ABO_3 structure, the larger cations Sr^{2+} and Ba^{2+} fit better. The size mismatch argument used here is a generalization of those used to justify the trends in thermal stability of salts containing polyatomic anions such as carbonate, nitrate, and sulfate.[33] In conclusion, the fact that $\Delta_{f,\text{oxides}}H_m^\circ$ becomes more negative from Ca to Ba reflects the combined effect of the different size mismatches in the ternary and the binary oxides.

In this context, it is interesting that $\Delta_{f,\text{oxides}}H_m^\circ$ for the cubic perovskites (Fig. 2) shows a minimum at Sr, and for this polymorph $\Delta_{f,\text{oxides}}H_m^\circ$ for $BaMnO_3$ is less negative than for $SrMnO_3$ since the Ba^{2+} ion is too large for the A-site environment of the undistorted cubic perovskite structure.

C. Corner- versus face-sharing octahedra

The formation of hexagonal perovskites is believed to be largely governed by the size misfits in the compound. While $BaMnO_3$ forms the 2*H*-hexagonal structure with face-sharing octahedra only, $CaMnO_3$ is orthorhombic and contains corner-sharing octahedra only. $SrMnO_3$ containing intermediately sized Sr ions takes the 4*H*-hexagonal structure which may be seen as intermediate containing both corner- and face-sharing octahedra. The hexagonal structures give more room to large alkaline-earth cations but, on the other hand, lead to short Mn-Mn distances connecting the centers of the face-sharing octahedra. While the distance between the manganese in two corner-sharing polyhedra in $SrMnO_3$ is 3.78 Å, the Mn-Mn distance over the common face is as short as 2.50 Å, and hence comparable to the Mn-Mn distance in metallic manganese (2.47 Å in γ-Mn). In $BaMnO_3$, the distance between these Mn atoms is even shorter (2.41 Å).[18] The face-sharing octahedra increase the electrostatic repulsion between the Mn atoms in the Mn_2O_9 entities, and therefore increase the magnitude of the Mn-Mn contribution to the Coulomb energy of the compound. The shortest O-O distance is in $BaMnO_3$ (both experimentally and in the calculations), consistent with the oxide ions moving to screen the repulsion, a point to which we return below.

In a previous study of ternary fluorides ABF_3 (*A*=Li-Cs, *B*=Mg-Ba) (Ref. 34) the corresponding transition from structures containing corner-sharing octahedra to hexagonal structures with face-sharing octahedra was modeled using a set of transferable potentials within the framework of the conventional ionic model. For every compound the lowest-energy structure was that experimentally observed. Since these calculations allow for no change in bonding from structure to structure and no ionic contributions, the driving force for the adoption of a structure by a given *fluoride* is clearly size. While in both series ABF_3 and $AMnO_3$, the transition from orthorhombic to cubic to hexagonal is consistent with the increase in the tolerance factor *t* [Eq. (1)] for each compound as the size of A^+ or A^{2+} increases, this very simple hard-sphere concept is quantitatively much more successful for the fluorides than for the oxides, presumably because of

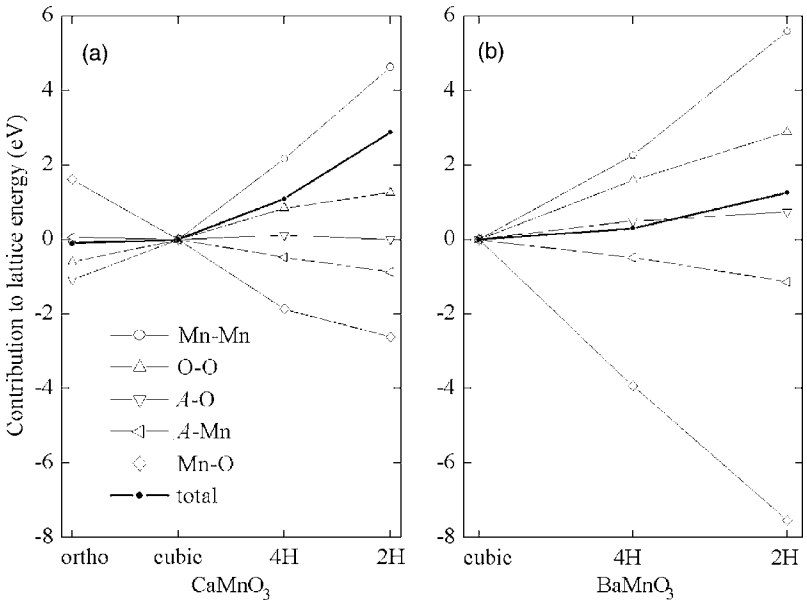

FIG. 8. The lattice energy decomposed into contributions (see insert to figure) for the different polymorphs considered for (a) $CaMnO_3$ and (b) $BaMnO_3$.

the greater ionicity of the fluorides. For the present oxides, the tolerance factor perform rather well, but it is clear that factors other than size also contribute. While the tolerance factor predict the cubic structure for $CaMnO_3$ (t=0.94), $SrMnO_3$ is found on the stability borderline between cubic and hexagonal (t=0.99). $BaMnO_3$ is predicted to adopt a hexagonal perovskite structure (t=1.06). We have here used the Shannon-Prewitt radii. However, for consistency with the work of Babel,[35] ionic radii for the 12-coordinate cations have been assumed to be 6% greater than the radii for the same ions when octahedrally coordinated.

In a purely ionic model the total energy is the lattice energy which can conveniently be separated into a Coulomb term and a term largely due to repulsion between the electron clouds on neighboring ions (the so-called Pauli repulsion),

$$E_{lattice} = \sum \left[\frac{q_i q_j}{4\pi\varepsilon_0 r_{ij}} + C \exp(-r_{ij}/\rho) \right], \tag{4}$$

where the summation is over any pair of ions i and j separated by r_{ij}. q_i is the charge, while C and ρ are constants. In the following discussion, we consider first the Coulomb energy due to long-range electrostatic interactions between the different ions represented as point charges and then indirectly the effects of other terms by considering bond-valence sums,[36,37] which are widely used in solid-state chemistry. These do not give energies directly but rather quantities which often correlate with energy. The bond-valence sum V_{ij} is the sum of all bond valences v_{ij} for bonds between two atoms i and j:

$$V_i = \sum_j v_{ij}. \tag{5}$$

The bond valence is a function of the distance d_{ij} between the two atoms and is given by

$$v_{ij} = \exp[(R_{ij} - r_{ij})/b]. \tag{6}$$

Here, b is a "universal" constant (0.37 Å) while R_{ij} is the bond-valence parameter. The latter is an empirical parameter for a given ion in a given oxidation state, derived from observed bond lengths for a large number of compounds. There is empirical evidence suggesting that the bond-valence sums for the elements in a given structure often correlates with the energy of that structure, and the lowest-energy structure is usually that in which the bond-valence sums are closest to the formal oxidation numbers of the given elements.

Significant information on the driving forces can, as indicated above, be obtained by an analysis of the main contributions to the Coulomb energy. The *ab initio* calculations have revealed the importance of covalent bonding in these compounds, and thus here we do not use the formal ionic model charges for the different ions but instead use the calculated average Bader charges: +1.6 for A, +2.0 for Mn, and −1.2 for O. We take interatomic distances from the calculated equilibrium geometries for the different structures. Figure 8 gives selected contributions to the Coulomb energy for $CaMnO_3$ and $BaMnO_3$. The Ca/Ba-O, Mn-O, Mn-Mn, Ca/Ba-Mn, and O-O contributions to the Coulomb energy are, for each compound, given relative to their contributions in the cubic modification of the compound.

Several features are worth noting. First of all, $CaMnO_3$ is orthorhombic; the orthorhombic deformation reduces the Ca-O distances and the Ca-O interactions become more favorable [Fig. 8(a)]. The 4H and 2H polymorphs have more unfavorable Coulomb energies. While the formation of the hexagonal structures gives more favorable Mn-O contributions to the lattice energy, the Mn-Mn and O-O distances become shorter and the energy penalty involved here is larger than the energy gain due to more favorable Mn-O interactions [Fig. 8(a)]. For $BaMnO_3$, the Coulomb energy itself favors the cubic modification [Fig. 8(b)]. Nevertheless, the gain in the Mn-O Coulomb energy (due to shorter Mn-O distances) contributes significantly to the stabilization of the

hexagonal structures. A comparison of Figs. 8(a) and 8(b) shows that the energy gain due to shorter Mn-O distances in the hexagonal polymorphs of $BaMnO_3$ (as shown by the open diamonds in both frames) is much more marked than for $CaMnO_3$ by a factor of 2–3, while the extra repulsion due to the shorter O-O and Mn-Mn distances (open circles and open triangles) is approximately comparable to $CaMnO_3$.

Clearly, factors other than the Coulomb energy stabilize the hexagonal polymorphs for $BaMnO_3$. The bond-valence sum empirically takes such factors into account and suggests that the 2*H*-hexagonal polymorph for $BaMnO_3$ is energetically favorable since both the Ba and Mn bond-valence sums for 2*H* $BaMnO_3$ are close to the formal oxidation numbers (1.9 and 3.9 for 2*H* compared with 2.4 and 3.7 for 4*H* and 3.1 and 3.4 for cubic). The bond-valence sum concept also gives results in agreement with experiment for $CaMnO_3$. Here, both structures based on corner-sharing octahedral have Ca and Mn bond-valence sums close to the formal oxidation numbers.

As mentioned earlier, the preference for hexagonal structures with increasing alkaline-earth cation size is often explained by metal-metal bonding.[38] In our previous study of 4*H*-hexagonal $SrMnO_3$ a charge-density analysis of the Mn_2O_9 dimer showed that the suggested Mn-Mn *d*-orbital overlap is small.[10] Instead, the charge density indicates covalent bonds between manganese and oxygen atoms, and these contribute to the stabilization of the hexagonal structures as the size of the alkaline-earth cation increases. In this context, it is significant that the Mn charge is much lower than the conventional ionic model charge due to the Mn-O covalence, and this reduces the Mn-Mn repulsion leading to sharing of the octahedral faces. We see no evidence for direct Mn-Mn metal bonding which has often been invoked to rationalize the adoption of this structure.

For the 4*H* polymorphs, the Mn and O ions relax from the "ideal" positions defined in Table III. In this ideal structure, the Mn ions are equally spaced and all Mn-O distances the same. For $CaMnO_3$, $SrMnO_3$, and $BaMnO_3$ each Mn atom is displaced approximately 0.011, 0.012, and 0.013 Å, respectively, from the ideal position along the *c* axis. The linking of the Mn_2O_9 units to neighboring octahedra by corner rather than face sharing makes possible a displacement of the Mn cations within the dimer units from the center of the octahedra and away from the shared face, thus reducing the electrostatic repulsion between them. In addition, the oxygen triangle in the shared face is significantly compressed, with O-O distances of 2.538, 2.517, and 2.481 Å (for A=Ca, Sr, and Ba, respectively), while the O-O distances in the plane where the octahedra share corners are 2.674, 2.745, and 2.847 Å, respectively, i.e., the difference between these increases from 0.14 to 0.23 and 0.37 Å for $CaMnO_3$, $SrMnO_3$, and $BaMnO_3$. The lower charge of the oxygen atoms in this face-sharing triangle (1.15 versus 1.27) contributes to the reduced O-O distances. The effect on the Coulomb energy is large. Figure 9 shows the changes in the total Coulomb energy and the changes in the contributions from Mn-O, Mn-Mn, *A*-O, and O-O interactions due to relaxation from the ideal 4*H* structure (see Table III). In the ideal structure, the O-O distances in the face-sharing triangle are comparable to the O-O distance in the corner-sharing layers. The Coulomb

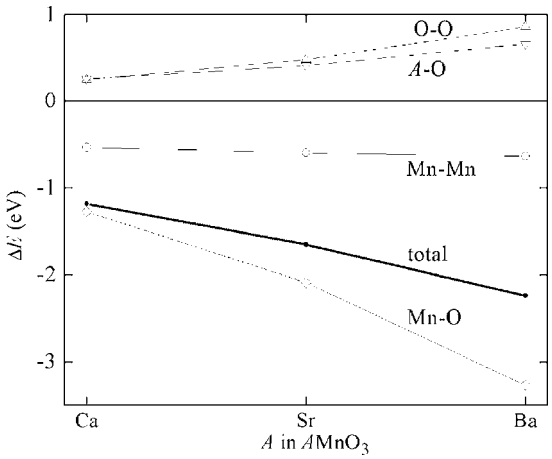

FIG. 9. The changes in Coulomb energy due to relaxation of the oxygen and manganese ions from the "ideal" positions of the 4*H* $AMnO_3$ structure. Details are given in the text.

energy gain from the relaxation increases as expected with the size of the *A* cation. While the O-O and *A*-O contributions raise the energy, the Mn-Mn and especially the Mn-O contributions lower the energy which in total becomes more favorable. In ideal 4*H* $SrMnO_3$ the Mn-O distance involving the face-sharing oxygens would be 1.952 Å compared to the observed value of 1.917 Å.

The polymorph stability is affected not only by the size of the *A*-site cation but also by temperature. Low-temperature 4*H*-type $SrMnO_3$ transforms to the cubic polymorph at 1035 °C. Similarly, 2*H*-type $BaMnO_3$ transforms to the 4*H* type through a series of hexagonal polymorphs between 1150 and 1550 °C.[9] Phase transitions in single-component systems are in general entropy driven. A simple first approximation rigidity argument[39,40] indicates a larger flexibility of octahedra sharing corners compared to octahedra sharing faces, and at a given temperature the entropy is expected to increase in the order $2H < 4H <$ cubic.

IV. SUMMARY

We have reported periodic *ab initio* calculations for perovskite-type $AMnO_3$, where A=Ca, Sr, and Ba, examining structures with corner and with face sharing of MnO_6 octahedra. The cubic, the 2*H*-, and the 4*H*-hexagonal modifications are examined for all three compounds. In addition, the orthorhombically distorted structure observed for $CaMnO_3$ is considered. Relative polymorph stability in agreement with experiment is obtained for all three compounds. Increasing the size of the alkaline-earth cation induces a transition from corner sharing to face sharing of octahedra. We have discussed the factors influencing the stability of the different polymorphs. The Mn charge is much lower than the conventional ionic model charge due to the Mn-O covalence, and this reduces the Mn-Mn repulsion and favors sharing of the octahedral faces. We see no evidence for direct Mn-Mn metal bonding which has often been invoked to rationalize the adoption of this structure.

We have, in addition, analyzed the variation of $\Delta_{f,\text{oxides}}H_m^o$ with the alkaline-earth cation for given polymorphs.

$\Delta_{f,\text{oxides}}H_m^o$ is often interpreted qualitatively in terms of factors related to oxide ion transfer between the constituent oxides, i.e., acidity/basicity. Here, we show that the variation in $\Delta_{f,\text{oxides}}H_m^o$ for the ternary oxides reflects largely the difference in lattice enthalpy of $A\text{MnO}_3$ and $(A\text{O}+\text{MnO}_2)$. $\Delta_{f,\text{oxides}}H_m^o$ for the $2H$ polymorph becomes more negative from Ca to Ba, which reflects the combined effect of the different size mismatches in the ternary and the binary oxides. Cation size can also be used to rationalize why $\Delta_{f,\text{oxides}}H_m^o$ for the *cubic* polymorphs shows a minimum at Sr. $\Delta_{f,\text{oxides}}H_m^o$ for BaMnO_3 is less negative than for SrMnO_3 since the Ba^{2+} ion is too large for the *A*-site environment of the undistorted cubic perovskite structure.

ACKNOWLEDGMENTS

This work was funded by the Research Council of Norway (Project No. 155117/432). The Research Council of Norway (Program for Supercomputing) has also supported the work through a grant of computing time.

*Corresponding author. Electronic address: svein.stolen@kjemi.uio.no

[1] R. D. Shannon and C. T. Prewitt, Acta Crystallogr., Sect. B: Struct. Crystallogr. Cryst. Chem. **25**, 925 (1969).
[2] F. F. Fava, P. D'Arco, R. Orlando, and R. Dovesi, J. Phys.: Condens. Matter **9**, 489 (1997).
[3] B. L. Chamberland, A. W. Sleight, and J. F. Weiher, J. Solid State Chem. **1**, 506 (1970).
[4] Y. Syono, S. I. Akimoto, and K. Kohn, J. Phys. Soc. Jpn. **26**, 993 (1969).
[5] T. Negas and R. S. Roth, J. Solid State Chem. **1**, 409 (1970).
[6] T. Negas, J. Solid State Chem. **7**, 85 (1973).
[7] L. Rørmark, A. B. Mørch, K. Wiik, S. Stølen, and T. Grande, Chem. Mater. **13**, 4005 (2001).
[8] T. Negas and R. S. Roth, J. Solid State Chem. **3**, 323 (1971).
[9] T. Negas, J. Solid State Chem. **6**, 136 (1973).
[10] R. Søndenå, P. Ravindran, S. Stølen, T. Grande, and M. Hanfland, Phys. Rev. B **74**, 144102 (2006).
[11] P. E. Blöchl, Phys. Rev. B **50**, 17953 (1994).
[12] P. Hohenberg and W. Kohn, Phys. Rev. **136**, B864 (1964).
[13] W. Kohn and L. J. Sham, Phys. Rev. **140**, A1133 (1965).
[14] G. Kresse and J. Furthmüller, Phys. Rev. B **54**, 11169 (1996).
[15] J. P. Perdew, K. Burke, and M. Ernzerhof, Phys. Rev. Lett. **77**, 3865 (1996).
[16] J. J. Adkin and M. A. Hayward, J. Solid State Chem. **179**, 70 (2006).
[17] A. J. Jacobson and A. J. W. Horrox, Acta Crystallogr., Sect. B: Struct. Crystallogr. Cryst. Chem. **32**, 1003 (1976).
[18] E. J. Cussen and P. D. Battle, Chem. Mater. **12**, 831 (2000).
[19] W. Gerlach, Z. Phys. A **9**, 184 (1922).
[20] J. S. Smart, Phys. Rev. **86**, 968 (1952).
[21] W. C. Mackrodt and E. A. Williamson, J. Chem. Soc., Faraday Trans. **93**, 3295 (1997).
[22] H. Taguchi, M. Sonoda, and M. Nagao, J. Solid State Chem. **137**, 82 (1998).
[23] T. Takeda and S. Ohara, J. Phys. Soc. Jpn. **37**, 275 (1974).
[24] P. D. Battle, T. C. Gibb, and C. W. Jones, J. Solid State Chem. **74**, 60 (1988).
[25] A. Hardy, Acta Crystallogr. **15**, 179 (1962).
[26] L. Rørmark, S. Stølen, K. Wiik, and T. Grande, J. Solid State Chem. **163**, 186 (2002).
[27] G. Henkelman, A. Arnaldsson, and H. Jónsson, Comput. Mater. Sci. **36**, 354 (2006).
[28] K. Terakura, T. Oguchi, A. R. Williams, and J. Kübler, Phys. Rev. B **30**, 4734 (1984).
[29] M. D. Towler, N. L. Allan, N. M. Harrison, V. R. Saunders, W. C. Mackrodt, and E. Aprà, Phys. Rev. B **50**, 5041 (1994).
[30] S. Stølen and T. Grande, *Chemical Thermodynamics of Materials: Macroscopic and Microscopic Aspects* (Wiley, New York, 2003).
[31] A. Navrotsky, Am. Mineral. **79**, 589 (1994).
[32] M. W. Chase, C. A. Davies, J. R. Downey, D. J. Frurip, R. A. McDonald, and A. N. Syverud, J. Phys. Chem. Ref. Data **14**, 1 (1985).
[33] D. A. Johnson, *Some Thermodynamic Aspects of Inorganic Chemistry*, 2nd ed. (Cambridge University Press, Cambridge, 1982).
[34] N. L. Allan, M. J. Dayer, D. T. Kulp, and W. C. Mackrodt, J. Mater. Chem. **1**, 1035 (1991).
[35] D. Babel, *Structure and Bonding* (Springer, Berlin, 1967).
[36] I. D. Brown, *The Chemical Bond in Inorganic Chemistry: The Bond Valence Model* (Oxford University Press, New York, 2002).
[37] N. E. Brese and M. O'Keeffe, Acta Crystallogr., Sect. B: Struct. Sci. **47**, 192 (1991).
[38] R. H. Mitchell, *Perovskites: Modern and Ancient* (Almaz Press, Thunder Bay, Canada, 2002).
[39] J. C. Phillips, J. Non-Cryst. Solids **34**, 153 (1979).
[40] J. C. Phillips, J. Phys.: Condens. Matter **16**, S5065 (2004).